Sub Topic: Combustion Theory and Modeling

12th U. S. National Combustion Meeting
Organized by the Eastern States Section of the Combustion Institute
May 24-26, College Station, Texas

Asymptotic Analysis of Premixed N-alkane Cool Flame Propagation

Vedha Nayagam[1*], Forman A. Williams[2], and Daniel L. Dietrich[3]

[1]*Department of Mechanical and Aerospace Engineering*
Case Western Reserve University, Cleveland, OH 44106, USA
[3]*Department of Mechanical and Aerospace Engineering, UCSD, La Jolla, CA 92093, USA*
[2]*NASA Glenn Research Center, Cleveland, OH 44135,USA*
[*]*Corresponding Author Email:* vedha.nayagam-1@nasa.gov

A simplified chemical-kinetic cool-flame mechanism for n-alkanes developed recently is applied to premixed laminar cool-flame deflagrations. The present contribution derives the structure of the associated freely propagating cool premixed flame controlled by the low-temperature chemistry and develops formulas for calculating the corresponding laminar burning velocity. Application of activation-energy asymptotics reveals finite-rate chemistry without heat release occurring throughout the preheat zone and leakage of both fuel and oxygen through the thin heat-release zone, there being zones of consumption of an intermediate species on each side of the heat-release zone, thicker than that zone but still thin compared with the preheat-zone thickness. Predicted laminar burning velocities are compared with recently reported measurements for n-dodecane, performed in a newly deigned high-pressure ignition apparatus, resulting in reasonable agreement.
Keywords: cool flames, premixed flame speed, n-alkanes, asymptotics

1. Introduction

The term cool-flame chemistry commonly is applied to the chemistry that occurs at temperatures within and below the temperature region (entirely below 1000 K) over which a negative temperature coefficient (NTC, induction time increasing with increasing temperature) is observed during autoignition of normal alkanes. In research motivated by measurements of the combustion and extinction of normal-alkane droplets supported by cool-flame chemistry [1], performed in the International Space Station (ISS), a maximally simplified chemical-kinetic description (developed beginning with the San Diego mechanism) was employed to describe the cool diffusion-flame structure and its extinction conditions [3]. That chemistry focused on n-heptane in air since n-heptane was the fuel investigated in most of the ISS experiments, but some measurements also were made with other normal alkanes, motivating later study of the applicability of the analysis to n-dodecane [4]. This last fuel is emphasized here because it is the fuel that was employed in recent ground-based experiments in which premixed cool-flame propagation was observed [5].

The cool diffusion flame is statically stable only if the heat-release rate in the reaction zone decreases with increasing temperature [6], as occurs in the NTC region, where there is competition between hot-flame and cool-flame chemistry. That decrease ends at a temperature below which the hot-flame chemistry no longer can compete with the cool-flame chemistry because it becomes too slow, whence the diffusion flame extinguishes there because it cannot be stable at temperatures below that limit. Premixed cool flames, similarly, will extinguish if the flame temperature falls below temperatures in the NTC range. The present work addresses propagation of premixed cool flames in the low-temperature portion of the NTC range, where the influence of the hot-flame chemistry can be ignored, so that the chemical kinetics introduced previously [3] can be simplified.

Cool flames have enjoyed a long history of scientific and engineering study. A thorough recent review documents these investigations [7]. Despite extensive experimental, computational, and theoretical work, relatively little is known about freely propagating, planar, steady-flow, premixed cool flames under adiabatic conditions, which are addressed here on the basis of low-temperature n-alkane chemistry. Interesting measurements have been made of cool-flame propagation in fuel-rich propane-oxygen mixtures, employing the low gravity levels achieved in aircraft flying parabolic trajectories [8]. All of the available steady-flow experiments, however, employ burners that are akin to flow reactors, either stabilized by the inlet or temperature-controlled by externally supplied side-wall heating or with ozone added to stabilize the flame [9]. Although useful for investigating flame structures, these steady-flow experiments did not provide laminar burning velocities without ozone addition and so cannot be compared with present predictions, which were developed in light of the previously mentioned recent experiments [5].

2. Chemistry

The chemical reactions in the present simplified description are shown in Table 1, where F denotes the normal alkane, R its alkyl radical, I the most relevant species resulting from the first oxygen addition to R (generally denoted as QOOH), and K the associated alkylketohydroperoxide. Here P and Q stand for collections of species that do not have to be considered. In this simplified description, following hydrogen abstraction from the original fuel by hydroxyl, the second step presumes rapid isomerization following the first oxygen addition. The third step is derived from steady-state approximations for the species formed by the second oxygen addition and for its isomerizations, resulting in maintaining partial equilibrium for its re-dissociation, and the fourth completes the low-temperature branching, having generated two hydroxyl radicals for the one initially consumed. The values of the rate parameters listed in the table are those that were termed "lumped" for n-dodecane in the previous publication [4].

The I removal by decomposition to hydropreoxyl and the conjugate alkene, the last step in the table, is found to be essential quantitatively. To properly describe extinction diameters in normal-alkane droplet combustion supported by cool-flame chemistry, a sixth step accounting for alkyl removal by high-temperature chemistry is needed as well, to achieve sufficient quantitative accuracy [3], but that chemistry is not included here because it plays no role in cool-flame deflagrations, which occur at flame temperatures in the NTC region but too low for hot-flame chemistry to be of importance. This chemistry then leads to a three-step formulation, rather than the four-step formulation found previously [3], when the facts that OH and R maintain steady states are introduced. Although this chemistry retains the dominant reaction-rate parameters, it does not reproduce correct cool-flame energetics. The heat release, which occurs largely at the rate of step 4, is dominated by subsequent consumption of products in the groups P and Q. That consump-

	Reaction	A	T_a
1	F+OH $\rightarrow$ R+H_2O	1.5 10^{12}	0
2	R+O_2 $\rightarrow$ I	3.7 10^{12}	0
3	I+O_2 $\rightarrow$ K+OH	6.4 10^{7}	-8360
4	K $\rightarrow$ P's+OH	6.0 10^{13}	19,840
5	I $\rightarrow$ Q's	3.0 10^{12}	12,090

Table 1: The elementary reactions and their rate coefficients in Arrhenius form $k = A\exp(-T_a/T)$ with rate parameters in mol, s, cm^3, and K.

tion appears to be fast enough that the associated rates are not relevant, whence only the product distribution requires consideration. Computationally, the products mainly are CO and H_2O, with lesser amounts of CH_2O and C_2H_4, but it is difficult to determine well what the distribution will be in premixed flames. Therefore the amount of heat release is considered to be an empirically adjustable parameter, the rate being that of step 4. Perhaps surprisingly, the value of the heat release turns out to influence predictions only to a minor extent (only by affecting the oxygen concentration mildly).

3. Formulation

The problem is formulated on the basis of conservation equations for mass, energy, and chemical species, the concentration $[i]$ of species i being related to its mass fraction Y_i according to $[i] = Y_i\rho/W_i$, where W_i is the molecular mass of species i, and ρ is the density of the gas. In the frame of reference of the propagating flame, with m denoting the constant total mass flow rate per unit area in that frame and D the thermal diffusivity of the mixture, the dimensionless streamwise coordinate ξ is taken to be the integral over distance of $m/(\rho D)$. With ω_j denoting the rate of step j in Table 1, after imposition of steady-state approximations for OH and R [3], the conservation equations for the remaining species become

$$\frac{\mathrm{d}Y_F}{\mathrm{d}\xi} = \frac{1}{L_F}\frac{\mathrm{d}^2Y_F}{\mathrm{d}\xi^2} - \frac{\rho D}{m^2}W_F\omega_4, \tag{1}$$

$$\frac{\mathrm{d}Y_O}{\mathrm{d}\xi} = \frac{\mathrm{d}^2Y_O}{\mathrm{d}\xi^2} - \frac{\rho D}{m^2}W_O\omega_4, \tag{2}$$

$$\frac{\mathrm{d}Y_I}{\mathrm{d}\xi} = \frac{1}{L_I}\frac{\mathrm{d}^2Y_I}{\mathrm{d}\xi^2} + \frac{\rho D}{m^2}W_I(\omega_4 - \omega_5), \tag{3}$$

$$\frac{\mathrm{d}Y_K}{\mathrm{d}\xi} = \frac{1}{L_K}\frac{\mathrm{d}^2Y_K}{\mathrm{d}\xi^2} + \frac{\rho D}{m^2}W_K(\omega_3 - \omega_4), \tag{4}$$

where L_i denoted the Lewis number of species i, the Lewis number of oxygen having been taken to be unity.

To simplify the expression for energy conservation, the specific heat at constant pressure is taken to be constant, and its product with W_KT_Q is defined as the heat release associated with step 4, that heat release being measured by the (empirical) temperature T_Q, the value of which (less than 100 K) is less than one one-hundredth of the value in the previous work [3], largely because of a revised (and more appropriate) normalization (the molecular weight W_K not having been

employed previously in the normalization). The differential equation for energy conservation then becomes

$$\frac{\mathrm{d}T}{\mathrm{d}\xi} = \frac{\mathrm{d}^2T}{\mathrm{d}\xi^2} + \frac{\rho D}{m^2} W_K T_Q \omega_4. \tag{5}$$

Boundary conditions are applied upstream (subscript u) at $\xi = -\infty$ and downstream (subscript f) at $\xi = \infty$. The values T_u, Y_{Fu}, and Y_{Ou} specify the mixture into which the flame is propagating, which may be lean, rich, or stoichiometric, with normal, diluted, or enriched air, while the intermediate mass fractions Y_I and Y_K must vanish at upstream infinity. The final temperature T_f is the flame temperature, which is approached at downstream infinity, but its value is determined by the flame structure and is not known in advance. Similarly, since both fuel and oxygen leak through the flame, the downstream values Y_{Ff} and Y_{Of} depend on the flame structure. The downstream boundary conditions for T and these leaking chemical species therefore are simply zero-gradient conditions, while the intermediate mass fractions Y_I and Y_K must vanish at downstream infinity, just as they do upstream.

4. Reaction Zones

Step 4 of Table 1 is seen to have the largest activation energy and therefore may be expected to occur in a thinner reaction zone than any of other other steps. It is appropriate to apply activation-energy asymptotics to this zone, and it is reasonable to employ $\epsilon = T_f^2/[T_a(T_f - T_u)]$ as the small parameter of expansion there, with T_a taken to be the activation temperature of step 4, having the large value 19,840 K (and the value of the prefactor of step 4 in Table 1 will later be denoted by A). It is convenient to place this thin reaction zone at $\xi = 0$ and to employ $\eta = \xi/\epsilon$ as the stretched independent variable to describe the structure of the zone. The heat release and production of the intermediate I are seen from (3) and (5) and the chemistry to occur in that zone, while fuel, oxygen, and the intermediate K are consumed there according to (1), (2), and (4). This is the heat-release zone because it is the only region in which chemical energy is released. Consistency of the analysis requires that Y_F and Y_O be of order unity in an expansion in ϵ in this zone, while Y_K and departures of T from T_f are of order ϵ.

Downstream from this thin reaction zone, to leading order Y_K is zero, and T, Y_F, and Y_O are constant, resulting in Y_I decaying unimolecularly, from its value, Y_{If}, in the thin reaction zone where it is produced, to zero at downstream infinity, with a constant value of the specific reaction-rate constant, at the rate of step 5; the relevant prefactor and activation temperature for step 5, appearing in Table 1, will be denoted by Q and T_q, respectively, the latter value being 12,090 K. The region over which this decay occurs may be thin compared with ξ but is thick compared with η, and matching to this solution at the thin reaction zone determines the gradient of Y_I to be applied there as a boundary condition for η approaching infinity.

Since $T_q < T_a$, both of which are large, upstream from the thin heat-release zone is a thicker diffusive-reactive zone in which step 5 consumes some of species I. This zone is thin compared with ξ, but variations of the intermediate I across it, along with proper matching, must be taken into account to obtain the correct boundary condition to apply for the concentration of I at $\xi = 0$ in considering the upstream region.

Upstream from these two thin reaction zones only step 3 occurs at leading order in the activation-energy asymptotics, so that the temperature and all species except K maintain a convective-diffusive balance. Species K is produced in a continuous manner in this region, at a rate that increases rapidly with decreasing temperature because of the effective large negative activation energy of step 3. Nevertheless the rate, being is proportional to Y_I, does vanish at upstream

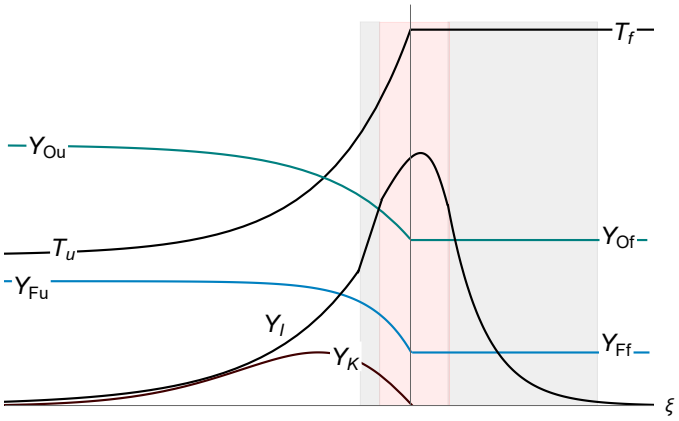

Figure 1: Schematic illustration of the reaction zones.

infinity, and, moreover, it does so exponentially with distance because of the exponential decay of Y_I that results from the convection-diffusion balance, whence integrations are convergent, no appeal being needed to initiation steps. In summary, then, there are four separate reaction regions in the present simplified model as illustrated schematically in figure 1

5. Downstream I Consumption

According to equation (3), for $\xi > 0$, where Y_K is small enough that ω_4 is negligible, all quantities remain constant except Y_I. If the rate of step 5 is fast enough that convection (the left-hand side) can be neglected, then the differential equation reduces to $\mathrm{d}^2Y_I/\mathrm{d}\xi^2 = b^2Y_I$, where the constant $b^2 = L_I\rho_f^2 D_f Q\mathrm{e}^{-T_q/T_f}/m^2$. The solution, subject to the boundary conditions, is simply $Y_I = Y_{If}\mathrm{e}^{-b\xi}$, which requires $L_I/b << 1$ for convection to remain negligible. The derivative of this provides, as a matching condition at $\xi = 0$ for the thin inner zone, $\mathrm{d}Y_I/\mathrm{d}\xi = -bY_{If}$. More generally, if convection is important in this zone, then this matching condition becomes $\mathrm{d}Y_I/\mathrm{d}\xi = -Y_{If}[(b^2 + L_I^2/4)^{1/2} - L_I/2]$, which will be employed in the analysis.

6. Heat-Release Zone

In applying activation-energy asymptotics to the thin heat-release zone, equations (4) and (5) have to be considered together, because the concentration of K appears in the rate of step 4. Since the convective terms are of higher order in this zone (and the rate of step 3 is negligible there), these two equations show that changes in Y_K there are L_K/T_Q times the changes in T. The useful dimensionless temperature-decrement variable for this zone is $z = (T_f - T)/[\epsilon(T_f - T_u)]$, and the integrations are performed by treating this rather than η as the independent variable. Since z and the scaled K mass fraction both vanish at infinity, the latter is $Y_K/\epsilon = L_K z(T_f - T_u)/T_Q$. At leading order, (5) then becomes the familiar equation $\mathrm{d}^2z/\mathrm{d}\eta^2 = \Lambda z\mathrm{e}^{-z}$, where the burning-rate eigenvalue is

$$\Lambda = \frac{T_f^4\rho_f^2 D_f L_K}{T_a^2(T_f - T_u)^2 m^2} A\mathrm{e}^{-(T_a/T_f)}, \tag{6}$$

in which, as previously indicated, A is the entry for step 4 in Table 1.
Integration of the differential equation for z shows that $\mathrm{d}z/\mathrm{d}\eta$ approaches $-\sqrt{2\Lambda}$ as η approaches $-\infty$, which is the matching condition needed for solving the energy equation in the upstream zone (convective-diffusive for T), providing a boundary condition at $\xi = 0$ for that

equation. This boundary condition, along with corresponding boundary conditions for other equations, may be summarized as

$$\frac{\mathrm{d}T}{\mathrm{d}\xi} = (T_f - T_u)\sqrt{2\Lambda}, \quad \frac{\mathrm{d}Y_O}{\mathrm{d}\xi} = -\frac{W_O(T_f - T_u)}{W_K T_Q}\sqrt{2\Lambda}, \quad \frac{\mathrm{d}Y_K}{\mathrm{d}\xi} = -\frac{L_K(T_f - T_u)}{T_Q}\sqrt{2\Lambda}, \quad (7)$$

and

$$\frac{\mathrm{d}Y_I}{\mathrm{d}\xi} = \frac{L_I W_I(T_f - T_u)}{W_K T_Q}\sqrt{2\Lambda} - [(b^2 + L_I^2/4)^{1/2} - L_I/2]Y_{If}, \quad (8)$$

to be applied at $\xi = 0$. The boundary condition for the fuel is not given here because the solution for its mass fraction in the upstream zone is not needed. The result of the matching given here for oxygen is obtained from the leading-order inner-zone differential equation derived from (2), in the same manner that the result for species K is derived from (4). Equation (3), for the intermediate I, is used in a similar way to derive the last result (8), making use of the matching condition as η approaches ∞, obtained from the solution in the downstream I-consumption region.

7. Upstream I Consumption

The small parameter of expansion in the narrow I-consumption region is $T_f^2/[T_q(T_f - T_u)]$. Since Y_I appears linearly in all terms, including the reaction term, its scaling does not affect the equations. At leading order in this zone Y_I remains Y_{If}; only its gradient changes. The change of the gradient is obtained from the integral of the reaction rate across the zone, that rate decreasing as ξ decreases because of the associated temperature decrease. The stretched independent variable ζ for this zone is defined as $-\xi$ divided by the small expansion parameter. For this zone, expansion of the Arrhenius factor about $T = T_f$ at leading order results in the differential equation $\mathrm{d}^2Y_I/\mathrm{d}\zeta^2 = cY_{If}\mathrm{e}^{-\zeta}$, where the constant $c = (\Lambda L_I T_a^2 Q\mathrm{e}^{-T_q/T_f})/(L_K T_q^2 A\mathrm{e}^{-T_a/T_f})$ and use has been made of (6). Integration of this equation from $\zeta = 0$ to $\zeta = \infty$ provides the change in the derivative across this zone, needed in matching to the preheat zone. This change, expressed in the ξ variable as the change in $\mathrm{d}Y_I/\mathrm{d}\xi$, is $cY_{If}T_q(T_f - T_u)/T_f^2$. Through matching of the solution in this zone to the solution for Y_I in the convective-diffusive zone, this last result, along with the boundary condition (8), then provides the boundary condition that is needed to complete the solutions for Y_I in all zones.

8. Preheat Region

Convective-diffusive balances apply for all species except K in the preheat region. The solution to equation (5) for the temperature is then simply

$$T = T_u + (T_f - T_u)\mathrm{e}^{\xi}. \quad (9)$$

Therefore, according to the first boundary condition in (7), Λ = 1/2, whence (6) provides an expression for the laminar burning velocity,

$$S_L = \frac{T_f^2\rho_f}{T_a(T_f - T_u)\rho_u}\sqrt{2L_K D_f A\mathrm{e}^{-(T_a/T_f)}}, \quad (10)$$

in which the value of T_f remains as an unknown.

It is convenient to express the solutions for the mass fractions of the species in terms of the temperature instead of ξ. Applying to equation (2) its boundary condition in (7) gives

$$Y_O = Y_{Ou} - (T - T_u)W_O/(W_K T_Q). \quad (11)$$

The convective-diffusive solution to equation (3) which satisfies the requirement that Y_I vanish at upstream infinity is proportional to $\mathrm{e}^{L_I\xi}$, which, in turn, clearly is proportional to $(T-T_u)^{L_I}$. At $\xi = 0$, where $Y_I = Y_{If}$, the derivative $\mathrm{d}Y_I/\mathrm{d}\xi$, obtained from matching to the slope of the upstream I-consumption zone, with use of Λ = 1/2 in (8), serves to determine the proportionality constant. The result is

$$Y_I = 2(T-T_u)^{L_I} W_I/[(1+C)W_K T_Q (T_f - T_u)^{L_I - 1}], \tag{12}$$

where the factor accounting for I consumption is

$$C = \frac{T_a^2 (T_f - T_u) Q \mathrm{e}^{-T_q/T_f}}{L_K T_q T_f^2 A \mathrm{e}^{-T_a/T_f}} + \left(1 + \frac{2T_a^2 (T_f - T_u)^2 Q \mathrm{e}^{-T_q/T_f}}{L_I L_K T_f^4 A \mathrm{e}^{-T_a/T_f}} \right)^{1/2}. \tag{13}$$

The source term for step 3 remains in equation (4) for Y_K which, with T as the independent variable, can be written as

$$(L_K - 1)\frac{\mathrm{d}Y_K}{\mathrm{d}T} = (T-T_u)\frac{\mathrm{d}^2 Y_K}{\mathrm{d}T^2} + \frac{W_K T_a^2 (T_f - T_u)^2 B \rho^3 D Y_O Y_I \mathrm{e}^{T_b/T}}{2W_O W_I T_f^4 \rho_f^2 D_f A \mathrm{e}^{-T_a/T_f}(T-T_u)}, \tag{14}$$

where T_b is 8360 K, the negative of the activation temperature for step 3 in Table 1, B is the pre-factor listed in the table for that step, and use has been made of equation 6 with Λ = 1/2. In the source term here, the factors that are variable have been written last, starting with ρ. This equation is to be solved subject to Y_K = 0 at $T = T_u$ and the last boundary condition in (7) at $T = T_f$. It is the further requirement that Y_K =0 at $T = T_f$ at leading order in this outer solution that finally determines the value of T_f.

The solution to the homogeneous form of (14) provides an integrating factor that can be used to solve the inhomogeneous equation. Application of the boundary conditions then ultimately results in the value of T_f being determined by a double integral, which can be integrated by parts to produce the single integral

$$\int_{T_u}^{T_f} \frac{W_K T_a^2 T_Q (T_f - T_u) B \rho^3 D Y_O Y_I \mathrm{e}^{T_b/T}}{2L_K W_O W_I T_f^4 \rho_f^2 D_f A \mathrm{e}^{-T_a/T_f}(T-T_u)} dT = 1. \tag{15}$$

Substitution of equations (11) and (12) into this equation and introduction of suitable approximations for the functional dependences of ρ and D, such as keeping their product constant and letting ρ vary inversely with T, then enables the integrals to be evaluated for guessed values of T_f, to be adjusted iteratively until this equality is satisfied. After that, the burning velocity can be calculated from equation (10).

The calculation of T_f as a function of T_u from equation (15) results in a double-valued function, exhibiting T_f values that decrease with increasing T_u (typically starting above 1000 K at T_u = 300 K), reaching a turning point (at T_u around 700 K), then decreasing further, asymptotically approaching T_u, as T_u is decreased from its turning-point value (where the temperature variations would become so slight that heat release would begin to extend throughout the entire flame structure, so a reasonably accurate thin heat-release zone no longer would exist). The turning point corresponds to the flame temperature reaching the low-temperature end of the NTC region. Since there is substantial leakage of reactants through the reaction zones of cool flames, those reaction zones behave in the same manner as homogeneous systems, and the finding [6] that the

diffusion flame is statically stable only in the NTC region applies equally well to the premixed flame. It follows that only the upper branch of the double-valued function is physically relevant; the flame would extinguish on the lower branch. The simplified chemical-kinetic description becomes increasingly accurate as the turning point is approached on the upper branch, but, lacking any high-temperature chemistry, it becomes increasingly inaccurate and eventually fails before the high-temperature end of the NTC region is reached, which occurs at a value of T_f around 900 K. The result is that the analysis cannot reasonable be extended to temperatures T_u below about 350 K or above about 650 K.

9. Aspects of the Predicted Burning Velocity

The assumption that the heat release occurs only in the thinnest reaction zone led to the burning velocity in equation (10) being determined by the flame temperature, without any explicit dependence on the heat-release parameter T_Q. That parameter appears indirectly in the integral (15) determining the flame temperature, although only through the oxygen mass fraction, as given in (11), since the product of T_Q with the mass fraction of species I may be seen from equations (12) and (13) to be independent of T_Q. Moreover, the predicted burning velocity is entirely independent of the fuel mass fraction Y_{Fu}, which may affect the results only to the extent that it modifies the value of T_Q, that is, only through its possible influence on the oxygen concentration profile. If oxygen depletion by the flame is negligible, then the burning velocity cannot depend on the initial fuel concentration (or on the heat release) according this this chemistry. This implies that the theory cannot be correct if the initial fuel concentration is too small. Further considerations of additional chemistry would be needed to address the question of when this failure occurs.
Since the burning velocity increases with increasing flame temperature at the higher flame temperatures, it increases with decreasing initial temperature, T_u at the lower values of T_u. The rapid variation with T_f of the Arrhenius factor in the denominator of equation (15) causes the difference $(T_f - T_u)$ to increase rapidly with increasing T_f, resulting in the calculated T_f increase with decreasing T_u. This increase of the flame temperature with decreasing initial temperature ultimately is a consequence of the negative activation energy of step 3. As T_u decreases, the rate of production of species K rapidly increases, so that there is a substantial increase of the rate of diffusion of K into the heat-release zone with this flame structure, causing the increase in the rate of heat release there and a consequent increase in T_f. Although it may be counterintuitive that burning velocities may increase with decreasing initial temperatures of the reactant mixture, the present flame structure, having finite-rate chemistry occurring throughout the preheat zone, causes that result to arise.

10. Comparisons of Predictions with Experiment

In the previously mentioned experiment [5], a droplet of n-dodecane, supported by a fiber, is quickly inserted into a furnace maintained at a fixed elevated temperature. The liquid begins to vaporize, and the vapor, being heavier than the surrounding gas, forms a downward-moving plume, traversing the path along which the droplet traveled (leaving vapor behind) during its insertion into the furnace. Cool-flame ignition first occurs in the lower part of this plume, where the residence time has been longest, and a premixed cool flame is observed to propagate upward, eventually reaching the droplet. The upward propagation velocity initially is constant, although later the flame accelerates. The difference between that initial upward velocity and the local gas velocity at the point and time of ignition may be considered to be the theoretically calculated burning velocity. Measurements were made at various pressures and furnace temperatures, and

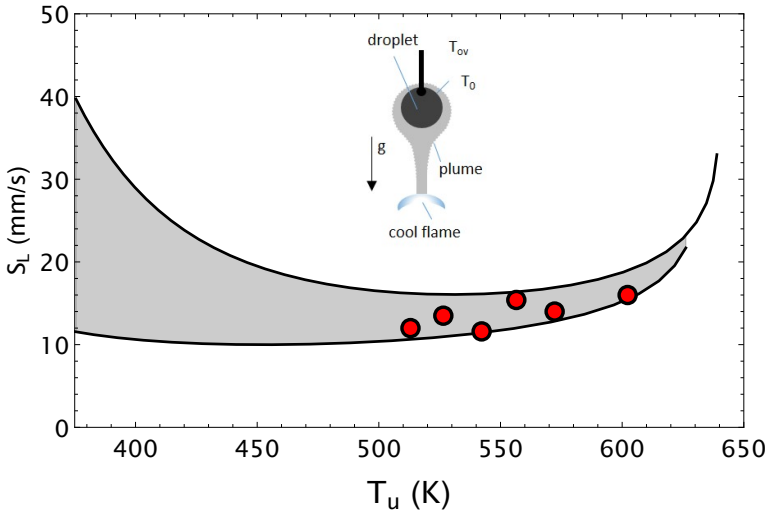

Figure 2: Theoretical (shaded region) and experimental (points) dependence of the burning velocity on the initial temperature at 3 atm for cool flames of n-dodecane in air.

those at 3 atm, for furnace temperatures from 558 K to 703 K, are compared with the calculated burning velocities in figure 2.

Local gas velocities at the point of ignition are uncertain in the experiment. Upward velocities imparted during the droplet-insertion process act against the downward plume velocities. in addition, random gas velocities that are not in the vertical direction are generated during insertion (as well as during heating prior to insertion). These are seen most clearly in the shadowgraphs at higher pressures, where the contrasts are greater, and they fall in the range of a few cm/s, comparable with calculated burning velocities (the normal-gravity experiments were merely workbench tests of an apparatus designed for microgravity experimentation in a drop tower, where residual velocities are damped prior to ignition, and a more quiescent condition is observed to be achieved). Because of these variations, the scatter in the experimental burning-velocity data is large, especially at pressures above 3 atm, and therefore the high-pressure data cannot be employed here. The scatter in the data shown in figure 2 is less than at higher pressures but is still evident.

A further experimental uncertainty stemming from the droplet insertion and vaporization concerns the gas temperature at the point and time of cool-flame ignition. The droplet is at 300 K prior to insertion, and it is heated and partially vaporized during insertion, as well as during the period of time between its arrival at its final position and cool-flame ignition. These processes will cause the gas temperature at the point and time of cool-flame ignition to be less than the furnace temperature. The furnace temperature for the two highest-temperature data points in figure 2 is, in fact, above the turning point of the theoretical curve, which emphasizes the importance of this effect. Since the transient nature of the variation of the temperature field precludes accurate determination of the gas temperature for any given point, in constructing the figure the temperature for each data point was simply taken to be one quarter of the sum of 300 K and three times the furnace temperature at the time of droplet insertion. This appears to be the best estimate that can be made, in view of the complexity of the processes occurring. The shaded region of figure 2 spans the range of Lewis numbers expected for species K. In earlier work, Lewis numbers of all carbon-containing species were takes to be 4, but, being even larger and heavier than the fuel

molecule, species I and K are likely to have a higher Lewis number than that. It is estimated that L_I and L_K lie between 4 and 6, and the upper bound of the shaded region is for $L_I = L_K = 4$, while the lower bound is for $L_I = L_K = 6$. The experimental data in the figure are seen to lie between these two bounds. In view of the very large uncertainties in both the property values employed in the computations and the experimental data, this extent of agreement seems noteworthy.

11. Conclusions

A maximally simplified cool-flame chemical-kinetic scheme, containing only five elementary steps, has been identified that results in a deflagration structure which, through activation-energy asymptotics, exhibits a thin heat-release zone, flanked on each side by a zone in which a key intermediate species (produced in the heat-release zone) is consumed, along with finite-rate production of a second key intermediate (from the first) throughout the preheat zone. Calculation of the laminar burning velocity from this description entails first calculating the flame temperature (determined by finite-rate chemistry with large amounts of reactant leakage) from a requirement that an integral (involving a reaction-rate ratio) across the flame structure be satisfied. When this is done, comparison of the predicted burning velocity with the only available measurements is found to be in agreement, within the (large) uncertainties of the properties and measurements.

References

[1] V. Nayagam, D. L. Dietrich, P.V. Ferkul, M. C. Hicks, and F. A. Williams. Can cool flames support quasi-steady alkane droplet burning? *Combustion and Flame*, 159:3583–3588, 2012.

[2] Forman A Williams and Vedha Nayagam. Quasi-steady combustion of normal-alkane droplets supported by cool-flame chemistry near diffusive extinction. *Combustion Theory and Modelling*, 23(4):748–770, 2019.

[3] Forman A Williams and Vedha Nayagam. Cool-flame dodecane-droplet extinction diameters. *Combustion and Flame*, 212:242–244, 2020.

[4] Evan N Rose, Vedha Nayagam, Daniel L Dietrich, Michael C Hicks, Uday G Hegde, Rosa E Padilla, and Forman A Williams. Autoignition dynamics of n-dodecane droplets under normal gravity. *Combustion Science and Technology*, 192:1–20, 2020.

[5] Guenter Paczko, Norbert Peters, Kalyanasundaram Seshadri, and Forman Arthur Williams. The role of cool-flame chemistry in quasi-steady combustion and extinction of n-heptane droplets. *Combustion Theory and Modelling*, 18(4-5):515–531, 2014.

[6] Yiguang Ju, Christopher B Reuter, Omar R Yehia, Tanvir I Farouk, and Sang Hee Won. Dynamics of cool flames. *Progress in Energy and Combustion Science*, 75:100787, 2019.

[7] Michael Foster and Howard Pearlman. Cool flame propagation speeds. *Combustion Science and Technology*, 179:1349–1360, 2007.

[8] M. Hajilou, M. Q. Brown, M. C. Brown, and E. Belmont. Investigation of the structure and propagation speeds of n-heptane cool flames. *Combustion and Flame*, 208:99–109, 2019.